

Effect of Cation Distribution and Structural Properties on Permeability of Ni-Mg Ferrite with Li_2CO_3 Additive

Mohammad Rabiul Hassan^{1,*}, Mohammad Torikul Islam², Mohammad Belal Hossain¹, Sumi Umme Honney¹, Mohammed Nazrul Islam Khan³

¹Physics Discipline, Khulna University, Khulna, Bangladesh

²Department of Physics, Hong Kong University of Science and Technology, Kowloon, Hong Kong

³Materials Science Division, Atomic Energy Centre, Dhaka, Bangladesh

Email address:

robifagun@yahoo.com (M. R. Hassan)

*Corresponding author

To cite this article:

Mohammad Rabiul Hassan, Mohammad Torikul Islam, Mohammad Belal Hossain, Sumi Umme Honney, Mohammed Nazrul Islam Khan. Effect of Cation Distribution and Structural Properties on Permeability of Ni-Mg Ferrite with Li_2CO_3 Additive. *Composite Materials*. Vol. 3, No. 1, 2018, pp. 1-8. doi: 10.11648/j.cm.20190301.11

Received: November 29, 2018; **Accepted:** January 16, 2019; **Published:** January 31, 2019

Abstract: The structural properties and permeability of polycrystalline $\text{Ni}_{0.6}\text{Mg}_{0.4}\text{Fe}_2\text{O}_4$ ferrite are studied with the addition of Li_2CO_3 at 0%, 2%, 4%, and 6%. The samples were synthesized by the conventional ceramic method at 1300°C sintering temperature for 6 hours. X-ray diffraction method is applied to understand the crystal structure of the following ferrite and it is confirmed that the samples have absolute single phase cubic spinel structure. The lattice constant of the ferrite varies with the increasing of Li_2CO_3 content. The microstructure analysis of the samples is carried out by SEM micrographs. From SEM images it is observed that the ferrite is in regular in shape and the grains are well connected with each other. The average grain sizes of the sample increased with increasing Li_2CO_3 content. Crystalline size of the sample follows the same manner of grain size of the samples. The Curie temperature is measured by using inductance analyzer. Curie temperature increased at 2% addition of Li_2CO_3 and the further increase in Li_2CO_3 leads to decrease in the Curie temperature whereas permeability shows just opposite attitude of Curie temperature in this study. Complex permeability and relative quality factor are also measured as a function of temperature and frequency respectively.

Keywords: Curie Temperature, Ferrite, Microstructure, Permeability

1. Introduction

Ferrite is a popular content in the earth of magnetism for its multifunctional uses. As metallic oxide, ferrite is also known as the ceramic material which has diverse applications in the field of electroceramics and magnetic memory. Ni-Mg ferrite has cubic spinel structure, considered as the face-centered cubic lattice (fcc), and most common type of magnetic material with AB_2O_4 [1] structure where the ions are dispersed in tetrahedral (A) and octahedral (B) lattice sites. For commercial importance, there has a great interest in the field of ferrite materials which enhances novel research on developing multifunctional ferrite materials. The Ni-Mg ferrite materials show spontaneous magnetization at below transition temperature which occurs for an anti-parallel arrangement of strongly coupled magnetic moments. Ni-Mg

ferrite has significant uses for its high electrical resistivity, low coercivity (i.e. soft ferrite), hardness, chemical stability, cost-effectiveness [2] etc that made more enthusiasm to manufacture ferrite materials at a large scale for industrial applications. The Ni-Mg ferrites are also popular for its high-frequency application and magneto-dielectric properties especially in microwave and radio frequency region [3]. In the low-frequency region, eddy current passes through ferrite materials, which causes the wastage of energy due to overheating [4]. Literature shows that the soft magnetic material has very low eddy loss [5].

On the other hand, the cation distribution of Ni-Mg depends on the preparation mechanism, sintering temperature and sintering time. In general, Mg ion occupies in both of

tetrahedral and octahedral sites for its inverse spinel structure whereas the Li and Ni ion occupy in tetrahedral and octahedral site respectively. Due to the addition of Li^{2+} ion in A site, few of Fe^{3+} ion are replaced from A site to B site. Some relevant works have done on Ni-Mg ferrite [2, 6, 7] and the effect of addition Li_2O on $\text{Ni}_{0.5}\text{Mg}_{0.5}\text{Fe}_2\text{O}_4$ ferrite already been studied [8]. But in this study, the proportion of Ni and Mg are 60% and 40% respectively which is distinctive from the study of Sheikh Mohi Uddin, *et al* [8]. It is expected that the presence of more Ni^{2+} than Mg^{2+} content on Ni-Mg alloy will help to increase magnetic properties. The domination of structural parameters on magnetic permeability is the main study area of the present research.

2. Procedures

2.1. Experimental Procedures

$\text{Ni}_{0.6}\text{Mg}_{0.4}\text{Fe}_2\text{O}_4$ with Li_2CO_3 additives (where $\text{Li}_2\text{CO}_3 = 0\%, 2\%, 4\%, 6\%$) are prepared by using double sintering method. The oxide materials NiO, MgO, Fe_2O_3 , and Li_2CO_3 with 99.99% purity (supplied by Sigma-Aldric) have been used in this experiment and weighing accurately by their molecular weight. All ingredients were mixed together by agate mortar for 12 hours and wet milled in ethyl alcohol for 6 hours. The samples were then dried in air at room temperature and the dried powder was pressed into disc shape in dies of 3 cm diameter. The discs were then pre-sintered in the air at 800°C for 3 hours. After the completion of pre-sintering, the samples were crushed again and wet milled in distilled water for 4 hours to obtain homogeneous and small crystallite size. The material was then dried and mixed with polyvinyl alcohol which helps to bind the powders for granulation. Then the powder was pressed into the ring by the ring shaped metal dies which outer and inner diameters are 1.30cm and 0.8cm respectively. Finally, the samples were sintered at 1300°C for 6 hours at $5^\circ\text{C}/\text{min}$ heating rate and cooled in air for 24 hours. The rings then polished by to make the surface regular. To smooth the surface of the ring, they are rubbed on the sandpapers.

2.2. Characterizations

The samples are characterized by X-ray diffractometer (Model: PW 3040-X'Pert PRO Philips) using $\text{CuK}\alpha$ radiation ($\lambda = 1.5405\text{\AA}$) at room temperature. Crystal structure of the sample is determined by using XRD data. Scanning electron microscope (SEM) is used to determine the microstructure of the sample. Permeability is measured at high-frequency Wayne Kerr 6500B impedance analyzer. Sample preparation and all characterizations are carried out in Atomic Energy Centre Dhaka (AECDC), Bangladesh.

3. Results and Discussion

3.1. XRD Analysis

The XRD patterns of $\text{Ni}_{0.6}\text{Mg}_{0.4}\text{Fe}_2\text{O}_4$ with the addition of

Li_2CO_3 are shown in “Figure 1” and it is seen that, the samples are belonging in the cubic spinel structure. All the Bragg reflections which guided the peaks are well-defined without any haziness. The absence of extra peaks is indicating the purity of samples where the peaks of different planes (220), (311), (222), (400), (422), (511) and (440) whatever odd or even, point out that the samples are in single spinel phase.

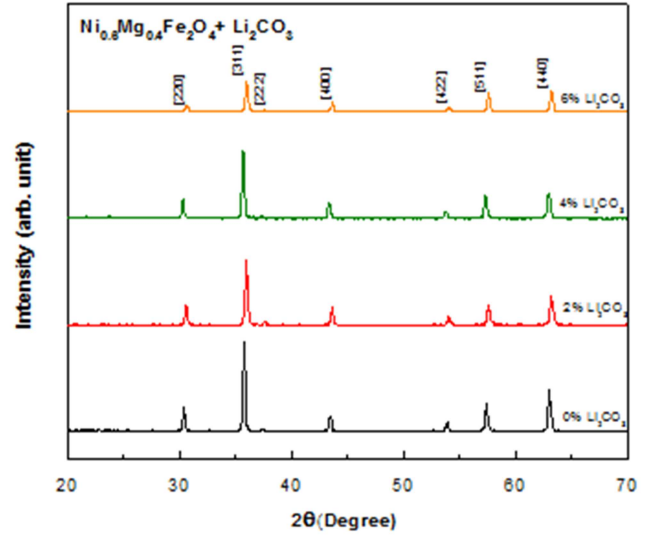


Figure 1. XRD pattern of $\text{Ni}_{0.6}\text{Mg}_{0.4}\text{Fe}_2\text{O}_4$ with Li_2CO_3 additives.

3.1.1. Cation Distribution and Calculation of Theoretical Lattice Parameter

The lattice parameters are calculated by using following equation:

$$a = d \times \sqrt{h^2 + k^2 + l^2} \quad (1)$$

Where, a is lattice parameter, d is mentioned as d -spacing of the ferrite crystal. When the corresponding Li^{2+} ions take place into A site, then the concentration of Fe^{3+} ion from A site is decreased. As a result, the concentration of Fe^{3+} increased into B site. Since the exchange of ions is not equilibrium at two constituent crystal sites, so the concentration of Fe^{3+} may be varied. In crystallographic spinel ferrite, the lattice parameter has been raising due to the correlation between the ionic radii of the octahedral and tetrahedral site. The theoretical lattice parameter is calculated by applying the following equation [9]:

$$a_{th} = \frac{8}{3\sqrt{3}} [(r_A + R_o) + \sqrt{3}(r_B + R_o)] \quad (2)$$

Where R_o , r_A and r_B are the ionic radii of oxygen ion (1.32\AA) [10], tetrahedral (A site) and octahedral (B site) sites respectively. The cation distribution is manipulated due to the variation r_A and r_B which influences spin alignment and magnetic properties of spinel ferrite. The cation distribution of Ni-Mg ferrite can be stated as follows:



Where () and [] brackets represent the A site and B site

respectively. The cations are distributed as:

1. Magnesium ferrite (MgFe_2O_4) is a partially inverted spinel ferrite, i.e.

$(\text{Mg}_{1-\lambda}\text{Fe}_\lambda)[\text{Mg}_\lambda\text{Fe}_{2-\lambda}]\text{O}_4$; where semi-circle and square brackets denote cation sites of tetrahedral (A-sites) and octahedral [B-sites] coordination, respectively [12].

2. On the other hand Li^{2+} and Ni^{2+} ions are partially entered in tetrahedral (A-sites) and octahedral [B-sites] sites respectively [13-14].

The value of r_A and r_B can be calculated by the following relations: [15-16]

$$r_A = C_{\text{AMg}}r(\text{Mg}^{2+}) + C_{\text{ALi}}r(\text{Li}^{2+}) + C_{\text{AFe}'}r(\text{Fe}^{3+}) \quad (3)$$

$$r_B = \frac{1}{2}[C_{\text{AMg}}r(\text{Mg}^{2+}) + C_{\text{BNi}}r(\text{Ni}^{2+}) + C_{\text{BFe}}r(\text{Fe}^{3+})] \quad (4)$$

Where the values of $r(\text{Mg}^{2+})$, $r(\text{Li}^{2+})$, $r(\text{Ni}^{2+})$ and $r(\text{Fe}^{3+})$ are (0.72\AA) , (0.76\AA) , (0.69\AA) and (0.645\AA) [15, 17, 18] respectively, while C_{AMg} , C_{ALi} and $C_{\text{AFe}'}$ are the concentration of Mg^{2+} , Li^{2+} , Fe^{3+} ions in A site and C_{BNi} and C_{BFe} are the concentration of Ni^{2+} and Fe^{3+} in B site.

The theoretical and experimental lattice parameters (a_{th} and a_{exp}) are plotted against Li_2CO_3 content in "Figure 2". From the graph it is shown that the a_{th} increased monotonically but a_{exp} is decreased at 2% addition of Li^{2+} content and after then the increasing in Li^{2+} causes to increase in a_{exp} . The a_{th} and a_{exp} for 0% addition of Li_2CO_3 content are 8.33\AA and 8.35\AA respectively. It is clearly observed that the values are close together which is raised due to the large porosity and density variance of the ferrite content. The rate of cation distribution is not same for both constituent lattice sites, which also is a driven force for the variation of lattice parameter.

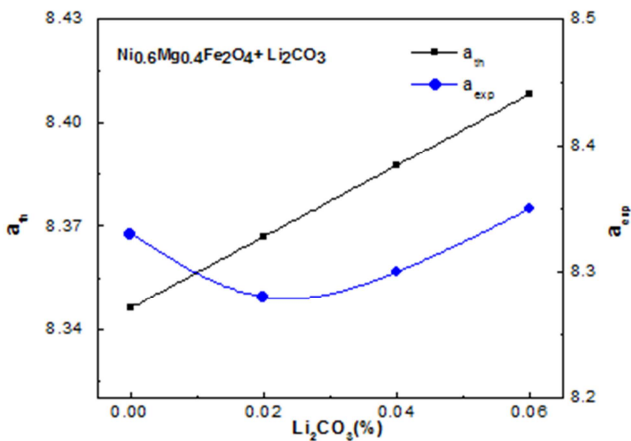


Figure 2. Variation of theoretical and experimental lattice parameter of $\text{Ni}_{0.6}\text{Mg}_{0.4}\text{Fe}_2\text{O}_4$ with Li_2CO_3 additives.

3.1.2. X-ray Density and Porosity

The x-ray density ρ_x is calculated by using molecular weight and the volume of the unit cell for individual sample is obtained by using the relation [18]

$$\rho_x = \frac{ZM}{Na^3} \quad (5)$$

Where M is the molecular weight, N is the Avogadro's number ($6.023 \times 10^{23} \text{ mole}^{-1}$), ' a ' is the lattice parameter and Z is the number of molecules per unit cell. The bulk density is calculated using the relation [19]:

$$\rho_B = \frac{m}{V} = \frac{m}{\pi r^2 h} \quad (6)$$

Where m is the mass of the pellet, r is the radius and h is the thickness. From the measured data it is observed that, the x-ray density is higher than the bulk density due to the pores in the crystal. From Table:1 it is shown that, the variation of densities and porosity are related with the variation of lattice parameter. At higher sintering temperature the grain growth usually irregular and this is developed due to intra-granular porosity and decrease in bulk density [20]. The porosity of the ferrite increased with increasing of Li_2CO_3 content as well.

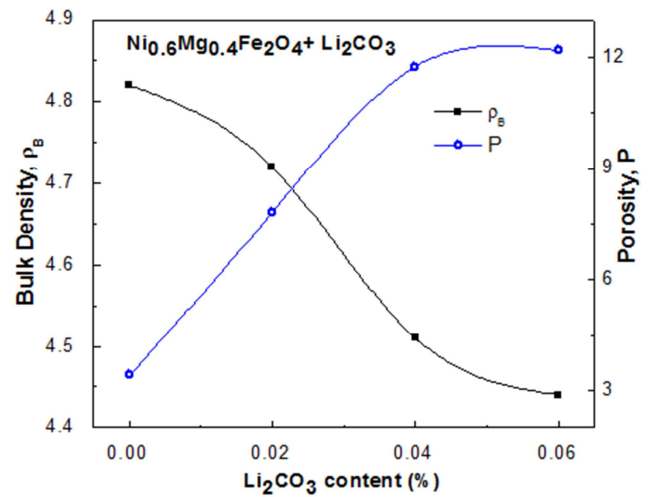


Figure 3. Bulk density and porosity of $\text{Ni}_{0.6}\text{Mg}_{0.4}\text{Fe}_2\text{O}_4$ with Li_2CO_3 additives.

The correlation between porosity and bulk density is shown in "Figure 3". The bulk density decreased with increasing Li_2CO_3 whereas x-ray density increased at 2% of Li_2CO_3 but decreased after adding more Li_2CO_3 which comply same agreement with the study on Ni-Mg ferrite by *M. M. Haque et al* [2]. The crystalline size of the samples is calculated by using Scherrer equation [19]

$$D = \frac{0.9\lambda}{\beta \cos \theta} \quad (7)$$

Where D is the mean crystalline size, λ is the X-ray wavelength, β is the FWHM, θ is the Bragg angle. The crystalline size decreased at 2% addition of Li_2CO_3 but further increasing of Li_2CO_3 leads to increase it and plotted in "Figure 4" in comparison with grain size.

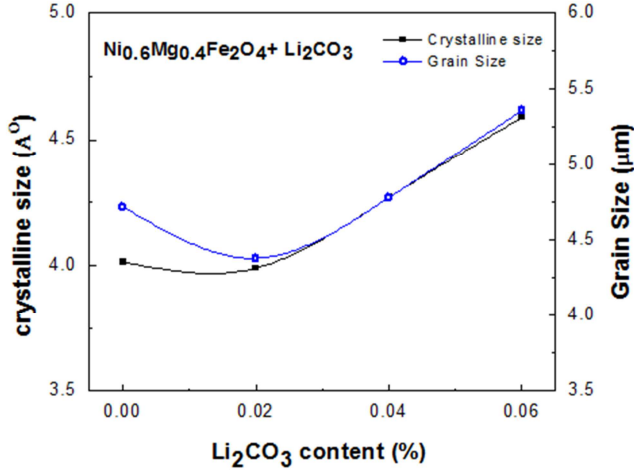


Figure 4. Variation in crystalline size and average grain size of $\text{Ni}_{0.6}\text{Mg}_{0.4}\text{Fe}_2\text{O}_4$ with Li_2CO_3 additives.

3.2. Microstructure

The Scanning Electron Microscope (SEM) was used to measure the average grain size and the micrographs are shown in “Figure 5”. The grain boundary mobilization and the intra-particle mass transportation are associated by the grain growth during sintering at higher temperature. The bimodal diffusion of grain has also been functionalized at sintering time [21, 22] which provokes the rate of grain growth. As the area of grain boundary decreases, the average grain size increased. From “Figure 5” it is observed that, the average grain size decreased at

2% Li_2CO_3 but increased at higher concentration of it.

Therefore when Li^{2+} was added to Ni-Mg ferrite, the pores inside grain boundaries being decreased which guided by intra-particle bimodal diffusion. The magnetic properties of ferrite materials are dominated by grain size and porosity. The net magnetization may be increased if the porosity is decreased inside the grain boundaries [21].

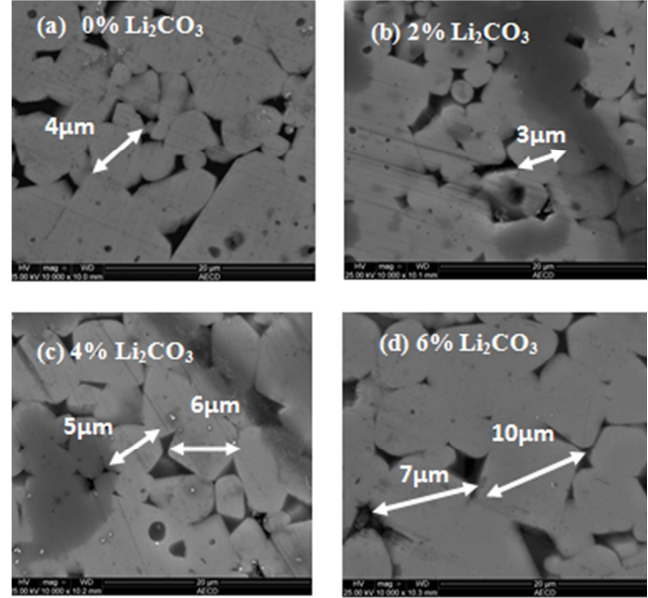


Figure 5. SEM micrographs of $\text{Ni}_{0.6}\text{Mg}_{0.4}\text{Fe}_2\text{O}_4$ with Li_2CO_3 additives.

Table 1. Ionic radius, theoretical & experimental lattice parameter, bulk & x-ray density, porosity.

No	Li_2CO_3 (%)	A site	B site	r_A (Å)	r_B (Å)	a_{th} (Å)	a_{exp} (Å)	ρ_B (gm/cm ³)	ρ_x (gm/cm ³)	Porosity (%)
01	0%	$(\text{Mg}_{0.05}^{2+}\text{Fe}_{0.95}^{3+})$	$[\text{Mg}_{0.45}^{2+}\text{Ni}_{0.5}^{2+}\text{Fe}_{1.05}^{3+}]\text{O}_4^{2-}$	0.649	0.673	8.35	8.33	4.82	4.99	3.41
02	2%	$(\text{Mg}_{0.05}^{2+}\text{Li}_{0.02}^{2+}\text{Fe}_{0.93}^{3+})$	$[\text{Mg}_{0.45}^{2+}\text{Ni}_{0.5}^{2+}\text{Fe}_{1.07}^{3+}]\text{O}_4^{2-}$	0.651	0.680	8.37	8.28	4.72	5.12	7.81
03	4%	$(\text{Mg}_{0.05}^{2+}\text{Li}_{0.04}^{2+}\text{Fe}_{0.91}^{3+})$	$[\text{Mg}_{0.45}^{2+}\text{Ni}_{0.5}^{2+}\text{Fe}_{1.09}^{3+}]\text{O}_4^{2-}$	0.653	0.686	8.39	8.3	4.51	5.11	11.74
04	6%	$(\text{Mg}_{0.05}^{2+}\text{Li}_{0.06}^{2+}\text{Fe}_{0.89}^{3+})$	$[\text{Mg}_{0.45}^{2+}\text{Ni}_{0.5}^{2+}\text{Fe}_{1.11}^{3+}]\text{O}_4^{2-}$	0.656	0.692	8.41	8.35	4.44	5.056	12.18

3.3. Field Dependence of Permeability

3.3.1. Frequency Dependent Real Part of Complex Permeability

Frequency dependent real part of complex permeability is given in “Figure 6”. The permeability is almost constant over 1 KHz ~ 12 MHz frequency range and the variation in the concentration of Li_2CO_3 has no significant effect on changing the permeability over that range of frequency. But at higher frequency, the permeability is started to fall in lower value though a small rise is experienced just before start to decreasing it. The permeability is given by:

$$\mu^* = \mu' - i \quad (8)$$

Where μ' and μ'' are known as real and imaginary part of complex permeability respectively.

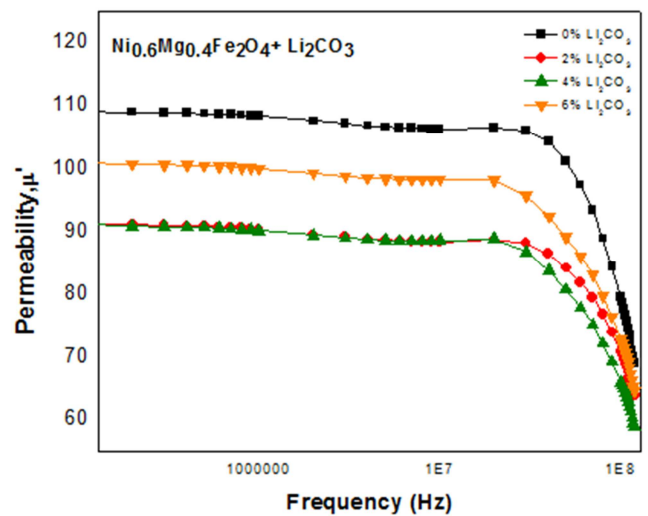


Figure 6. Change in real permeability with frequency changes of $\text{Ni}_{0.6}\text{Mg}_{0.4}\text{Fe}_2\text{O}_4$ with Li_2CO_3 additives.

The dispersion in domain wall motion and spin rotation are

experienced due to the change in frequency from lower to higher order whereas permeability is dominated by these effects [23, 24].

On the other hand initial permeability is decreased after increasing the concentration of Li_2CO_3 but the higher concentration of Li_2CO_3 leads to increase it. So the decrease in permeability with higher value of frequency attributed ferromagnetic resonance [25] which has the similarity with Snoek's relation i.e. $f_r \mu' = \text{constant}$, where f_r is the resonance frequency [26].

3.3.2. Frequency Dependence of Relative Quality Factor (RQF)

From "Figure 7" it is observed that the relative quality factor (RQF) increases with increasing frequency and after generating a characteristic peak, it decreased.

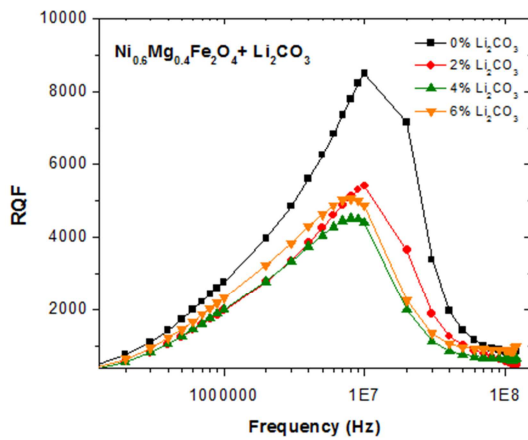


Figure 7. The variation in relative quality factor (RQF) with frequency changes of $\text{Ni}_{0.6}\text{Mg}_{0.4}\text{Fe}_2\text{O}_4$ with Li_2CO_3 additives.

Several defects [27] like non-uniform, non-repetitive domain wall motion, domain wall bowing, variation of magnetic flux densities, nucleation and annihilation of domain wall [28] are responsible for the reduction in RQF. The rapid decrease in RQF is happened at the maximum resonance energy which is shifted from the applied magnetic field to the lattice and this fact is related with the ferromagnetic resonance within the domain. The quality factor is a parameter of measuring the performance for practical application. The highest Q value of $\text{Ni}_{0.6}\text{Mg}_{0.4}\text{Fe}_2\text{O}_4$ is found to be 8.495×10^3 at 0% addition of Li_2CO_3 .

3.4. Temperature Dependence of Permeability

3.4.1. Measurement of Curie Temperature (T_C) and Temperature Dependence of Permeability

"Figure 8" shows the variation in permeability of $\text{Ni}_{0.6}\text{Mg}_{0.4}\text{Fe}_2\text{O}_4$ with the change in temperature at different Li_2CO_3 additives and from this figure it is seen that the initial permeability decreases at 2% in Li_2CO_3 content but further increasing in Li_2CO_3 content leads to increase in permeability.

At Curie temperature the ferromagnetic material changed into paramagnetic material i.e. the magnetically

ordered materials turned out to be magnetically disorder [2, 14, 29]. The initial permeability increases with increasing in temperature and reached maximum value just before Curie temperature. At the ferro-paramagnetic transition phase, the initial permeability is fallen sharply to very lower value. The strength of exchange interaction among the magnetic atom can also be described in association of Curie temperature.

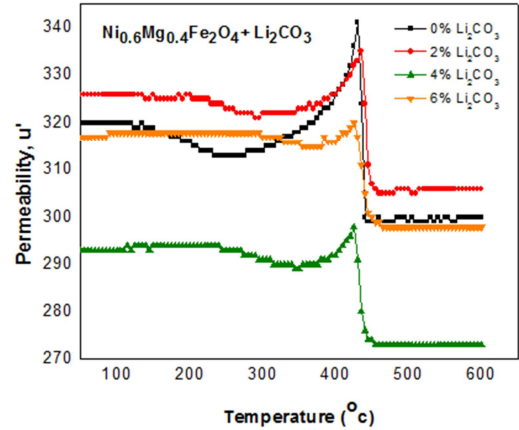


Figure 8. The variation in permeability with temperature changes of $\text{Ni}_{0.6}\text{Mg}_{0.4}\text{Fe}_2\text{O}_4$ with Li_2CO_3 additives.

The magnitude of initial permeability μ' is proportional to the square of initial permeability and inversely proportional to the magnetic magneto-crystalline anisotropy constant [14] also known as Globus et al. relation [15] which can be written as:

$$\mu' = \frac{M_s^2 D}{\sqrt{\kappa_1}} \quad (9)$$

Where M_s is the saturation magnetization, D is the average grain size and κ_1 is the anisotropy constant. The saturation magnetization (M_s) and the anisotropy constant (κ_1) usually decrease with increase in temperature [28] and the variation in permeability can be described with these factors. The rate of decreasing in κ_1 is much faster than decrease in M_s with temperature [30] which provides to increase in permeability.

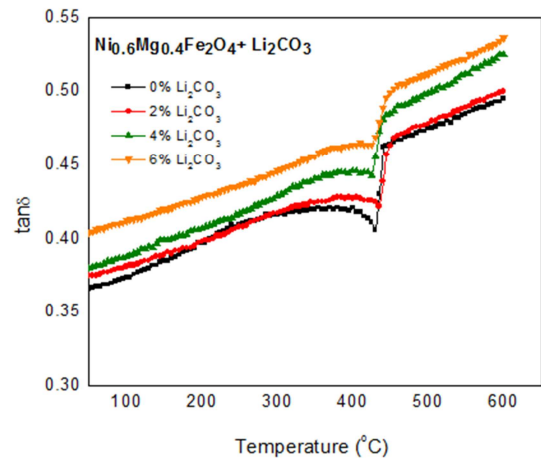


Figure 9. The variation in loss tangent with temperature changes of $\text{Ni}_{0.6}\text{Mg}_{0.4}\text{Fe}_2\text{O}_4$ with Li_2CO_3 additives.

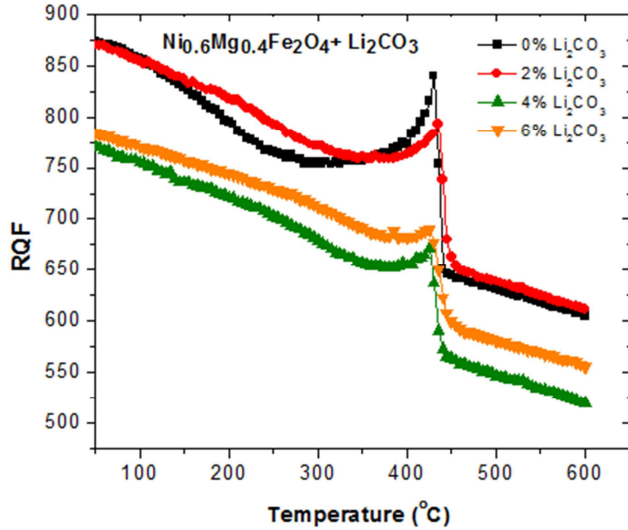


Figure 10. The variation in RQF with temperature changes of $\text{Ni}_{0.6}\text{Mg}_{0.4}\text{Fe}_2\text{O}_4$ with Li_2CO_3 additives.

The change in loss tangent ($\tan\delta$) and relative quality factor (RQF) with the variation of Li^{2+} content as the function of temperature are shown in “Figure 9” and “Figure 10” respectively. It is observed that, the increasing in Li^{2+} content involves increasing in loss tangent but plays a

significant tool to decrease in RQF. Similarly when temperature increases, the loss also increased but RQF decreased and from this statement it is assumed that the loss tangent and RQF have opposite characteristics of each other.

A sharp fall is experienced for both in loss tangent and RQF plot in Curie temperature region which has almost same agreement with the study of permeability. “Figure 11” shows the change in Curie temperature with the variation of Li_2CO_3 concentration. From this graph we assumed that the Curie temperature of the material suddenly increased at 2% increasing of Li_2CO_3 but further increasing in the content concentration the Curie temperature decreased. “This characteristic may be ascribed by the modification of A-B exchange interaction due to the addition of Li_2CO_3 which already described in previous section. When 2% of Li_2CO_3 was added then the sudden increase in Li^{2+} ion leads to increase in Curie temperature. Hence the number of Fe^{3+} ions is not balanced among two sites but further increasing in Li^{2+} on A site causes to increase of Fe^{3+} ions in B site. In that case J_{AA} becomes weaker and contributes in the weakening of the strength of J_{AB} exchange interaction which leads to decrease in Curie temperature.

Table 2. Average Grain Size, Crystalline Size of $\text{Ni}_{0.6}\text{Mg}_{0.4}\text{Fe}_2\text{O}_4$ with Li_2CO_3 additives.

No	Li_2CO_3 (%)	Average Grain Size μm	Crystalline Size \AA	Curie Temperature T_C ($^\circ\text{C}$)	Initial Permeability μ'
1	0%	4.72	4.0135	429	196
2	2%	4.38	3.9887	434	174
3	4%	4.78	4.2677	425	179
4	6%	5.36	4.5888	420	180

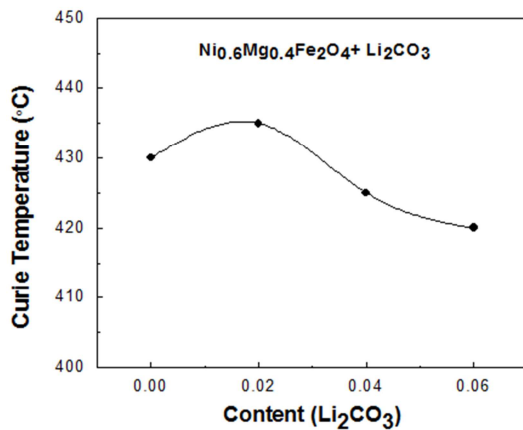


Figure 11. The variation in Curie temperature of $\text{Ni}_{0.6}\text{Mg}_{0.4}\text{Fe}_2\text{O}_4$ with Li_2CO_3 additives.

“Figure 12” shows the variation in initial permeability with the variation of Li_2CO_3 content. From this graph it is manifested that the initial permeability decreases at 2% increasing of Li_2CO_3 and further increase in content involves increasing in initial permeability. Furthermore it has the same agreement stated in the Globus and Duplex model [31],

where the permeability depends on the formation of microstructure. It is already discussed that the large grain size contributes in higher domain wall motion and for this reason the permeability reached the higher value. The decreasing in density also causes to increase in pores inside the intra-granular region which resulting to increase in the rate of demagnetization and reduces the spin rotational contribution [32, 33]. Therefore the permeability decreased.

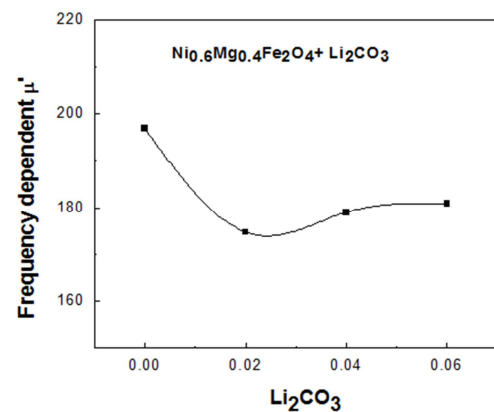


Figure 12. The variation in initial permeability of $\text{Ni}_{0.6}\text{Mg}_{0.4}\text{Fe}_2\text{O}_4$ with Li_2CO_3 additives.

4. Conclusion

The structural and physical properties of $\text{Ni}_{0.6}\text{Mg}_{0.4}\text{Fe}_2\text{O}_4$ with the addition of Li_2CO_3 are successfully studied by x-ray diffraction method and SEM technique where the material was synthesized by conventional ceramic method at 1300°C sintering temperature for 6 hours. The lattice parameter and grain size were increased and the bulk density and x-ray density decreased with increasing of Li_2CO_3 content on the Ni-Mg ferrite. On the other hand, the grain size of the samples was increased with increasing Li_2CO_3 content which may be considered as the same consequence of XRD data. From these data it is concluded that there has no impurity and segregation on the sample. The initial permeability decreased at 2% Li_2CO_3 and then increased whereas the Curie temperature increased at 2% Li_2CO_3 and then decreased. As for both in frequency and temperature, the loss tangent has increased but RQF has decreased although the Li^{2+} content was increased in Ni-Mg ferrite.

Acknowledgements

The paper is written on the basis of academic research work of Physics Discipline, Khulna University, Bangladesh. All samples were prepared in the Material Science laboratory of Atomic Energy Centre, Dhaka Bangladesh. We are grateful to both institutions for their support.

References

- [1] Hashim, Mohd, Shalendra Kumar, Sagar E. Shirsath, R. K. Kotnala, Jyoti Shah, and Ravi Kumar. "Influence of Cr^{3+} ion on the structural, ac conductivity and magnetic properties of nanocrystalline Ni-Mg ferrite." *Ceramics International* 39, no. 2 (2013): 1807-1819.
- [2] Haque, Md Mahbubul, Kazi Haniun Maria, Shamima Choudhury, Mahabub Alam Bhuiyan, and M. A. Hakim. "Synthesis, microstructure and magnetic properties of Ni-Mg ferrites." *J. Ceram. Process. Res* 14 (2013): 82-86.
- [3] Belavi, P. B., G. N. Chavan, L. R. Naik, R. Somashekar, and R. K. Kotnala. "Structural, electrical and magnetic properties of cadmium substituted nickel-copper ferrites." *Materials Chemistry and Physics* 132, no. 1 (2012): 138-144.
- [4] Muthuraman, K., Vasant Naidu, S. K. A. Ahmed, and T. Vasudevan. "Study of electrical and magnetic properties of cerium doped nano smart magnesium ferrite material." *International Journal of Computer Applications* 65, no. 23 (2013).
- [5] Shokrollahi, H., and K. Janghorban. "Soft magnetic composite materials (SMCs)." *Journal of Materials Processing Technology* 189, no. 1-3 (2007): 1-12.
- [6] El Hiti, M. A. "AC electrical conductivity of Ni-Mg ferrites." *Journal of Physics D: Applied Physics* 29, no. 3 (1996): 501.
- [7] Mittal, V. K., P. Chandramohan, Santanu Bera, M. P. Srinivasan, S. V. N. S. Velmurugan, and S. V. Narasimhan. "Cation distribution in $\text{Ni}_x\text{Mg}_{1-x}\text{Fe}_2\text{O}_4$ studied by XPS and Mössbauer spectroscopy." *Solid state communications* 137, no. 1-2 (2006): 6-10.
- [8] Rummy, Sheikh Mohi Uddin, Mahabub Alam Bhuiyan, MH Mesbah Ahmed, Kazi Haniun Maria, M. A. Hakim, D. K. Saha, and Shamima Choudhury. "Effects of Li_2O additive on structural, magnetic and electrical properties of Ni-Mg ferrite." *Journal of Bangladesh Academy of Sciences* 38, no. 1 (2014): 7-18.
- [9] Mazen, S. A., M. H. Abdallah, R. I. Nakhla, H. M. Zaki, and F. Metawe. "X-ray analysis and IR absorption spectra of Li-Ge ferrite." *Materials chemistry and physics* 34, no. 1 (1993): 35-40.
- [10] Tereshina, E. A., and A. V. Andreev. "Crystal structure and magnetic properties of $\text{Lu}_2\text{Co}_{17-x}\text{Si}_x$ single crystals." *Intermetallics* 18, no. 4 (2010): 641-648.
- [11] Pradhan, S. K., S. Bid, M. Gateshki, and V. Petkov. "Microstructure characterization and cation distribution of nanocrystalline magnesium ferrite prepared by ball milling." *Materials Chemistry and Physics* 93, no. 1 (2005): 224-230.
- [12] Franco Jr, A., and M. S. Silva. "High temperature magnetic properties of magnesium ferrite nanoparticles." *Journal of Applied Physics* 109, no. 7 (2011): 07B505.
- [13] Walz, Friedrich. "The Verwey transition-a topical review." *Journal of Physics: Condensed Matter* 14, no. 12 (2002): R285.
- [14] Hongzhi, Luo, Zhu Zhiyong, Ma Li, Xu Shifeng, Liu Heyan, Qu Jingping, Li Yangxian, and Wu Guangheng. "Electronic structure and magnetic properties of Fe_2YSi (Y= Cr, Mn, Fe, Co, Ni) Heusler alloys: a theoretical and experimental study." *Journal of Physics D: Applied Physics* 40, no. 22 (2007): 7121.
- [15] Mandal, K., S. Pan Mandal, P. Agudo, and M. Pal. "A study of nanocrystalline (Mn-Zn) ferrite in SiO_2 matrix." *Applied surface science* 182, no. 3-4 (2001): 386-389.
- [16] Li, Feng, Junjie Liu, David G. Evans, and Xue Duan. "Stoichiometric synthesis of pure MFe_2O_4 (M= Mg, Co, and Ni) spinel ferrites from tailored layered double hydroxide (hydrotalcite-like) precursors." *Chemistry of Materials* 16, no. 8 (2004): 1597-1602.
- [17] Li, Feng, Junjie Liu, David G. Evans, and Xue Duan. "Stoichiometric synthesis of pure MFe_2O_4 (M= Mg, Co, and Ni) spinel ferrites from tailored layered double hydroxide (hydrotalcite-like) precursors." *Chemistry of Materials* 16, no. 8 (2004): 1597-1602.
- [18] Modi, K. B., M. K. Rangolia, M. C. Chhantbar, and H. H. Joshi. "Study of infrared spectroscopy and elastic properties of fine and coarse grained nickel-cadmium ferrites." *Journal of materials science* 41, no. 22 (2006): 7308-7318.
- [19] Nam, J-H., W-G. Hur, and J-H. Oh. "The effect of Mn substitution on the properties of NiCuZn ferrites." *Journal of applied physics* 81, no. 8 (1997): 4794-4796.
- [20] Ajmal, Muhammad, and Asghari Maqsood. "Structural, electrical and magnetic properties of $\text{Cu}_{1-x}\text{Zn}_x\text{Fe}_2\text{O}_4$ ferrites ($0 \leq x \leq 1$)." *Journal of Alloys and Compounds* 460, no. 1-2 (2008): 54-59.
- [21] Belavi, P. B., G. N. Chavan, L. R. Naik, R. Somashekar, and R. K. Kotnala. "Structural, electrical and magnetic properties of cadmium substituted nickel-copper ferrites." *Materials Chemistry and Physics* 132, no. 1 (2012): 138-144.

- [22] Charalambous, Harry, Shikhar Krishn Jha, Kent Harrison Christian, Ryan Thomas Lay, and Thomas Tsakalakos. "Flash sintering using controlled current ramp." *Journal of the European Ceramic Society* 38, no. 10 (2018): 3689-3693.
- [23] Caltun, O. F., L. Spinu, Al Stancu, L. D. Thung, and W. Zhou. "Study of the microstructure and of the permeability spectra of Ni-Zn-Cu ferrites." *Journal of Magnetism and Magnetic Materials* 242 (2002): 160-162.
- [24] Nakamura, T., T. Tsutaoka, and K. Hatakeyama. "Frequency dispersion of permeability in ferrite composite materials." *Journal of magnetism and magnetic materials* 138, no. 3 (1994): 319-328.
- [25] Verma, Anjali, and Ratnamala Chatterjee. "Effect of zinc concentration on the structural, electrical and magnetic properties of mixed Mn-Zn and Ni-Zn ferrites synthesized by the citrate precursor technique." *Journal of magnetism and magnetic materials* 306, no. 2 (2006): 313-320.
- [26] Nikmanesh, Hossein, Sedigheh Hoghoghifard, and Behnaz Hadi-Sichani. "Study of the structural, magnetic, and microwave absorption properties of the simultaneous substitution of several cations in the barium hexaferrite structure." *Journal of Alloys and Compounds* 775 (2019): 1101-1108.
- [27] Dawoud, Hussain, and Sami Shaat. "Magnetic properties of Zn substituted Cu ferrite." *An-Najah Univ. J. Res.(N. Sc.)* 20 (2006): 87-100.
- [28] Maaz, K., S. Karim, A. Mumtaz, S. K. Hasanain, J. Liu, and J. L. Duan. "Synthesis and magnetic characterization of nickel ferrite nanoparticles prepared by co-precipitation route." *Journal of Magnetism and Magnetic Materials* 321, no. 12 (2009): 1838-1842.
- [29] Maria, Kazi Hanium, Shamima Choudhury, and Mohammad Abdul Hakim. "Structural phase transformation and hysteresis behavior of Cu-Zn ferrites." *International Nano Letters* 3, no. 1 (2013): 42.
- [30] Nath, Suman Kumar, Kazi Hanium Maria, Saroaut Noor, S. S. Sikder, S. Manjura Hoque, and M. A. Hakim. "Magnetic ordering in Ni-Cd ferrite." *Journal of Magnetism and Magnetic Materials* 324, no. 13 (2012): 2116-2120.
- [31] A. Globus, P. Duplex, *IEEE Trans. Magn. Mag-2.* 3 (1996)441-445.
- [32] Shrotri, J. J., S. D. Kulkarni, C. E. Deshpande, A. Mitra, S. R. Sainkar, PS Anil Kumar, and S. K. Date. "Effect of Cu substitution on the magnetic and electrical properties of Ni-Zn ferrite synthesised by soft chemical method." *Materials Chemistry and Physics* 59, no. 1 (1999): 1-5.
- [33] Mahmud, S. T., AKM Akther Hossain, AKM Abdul Hakim, M. Seki, T. Kawai, and H. Tabata. "Influence of microstructure on the complex permeability of spinel type Ni-Zn ferrite." *Journal of Magnetism and Magnetic Materials* 305, no. 1 (2006): 269-274.